Nanoscale Advances

ROYAL SOCIETY OF CHEMISTRY

PAPER

View Article Online
View Journal | View Issue

Cite this: *Nanoscale Adv.*, 2025, **7**, 1803

High-performance boron nitride/graphene oxide composites modified with sodium thiosulfate for energy storage applications

Shamsiya Shams,†[a] B. Bindhu,*[a] Adhigan Murali,†[b] R. Ramesh, *[c] Abdullah Al Souwaileh[d] and Sung Soo Han*[b]

Two-dimensional (2D) hybrid materials, particularly those based on boron nitride (BN) and graphene oxide (GO), have attracted significant attention for energy applications owing to their distinct structural and electronic properties. BN/GO composites uniquely combine the mechanical strength, thermal stability and electrical insulation of BN with the high conductivity and flexibility of GO, creating advanced materials ideal for the fabrication of batteries, supercapacitors and fuel cells. These hybrids offer synergistic effects, enhanced charge transport, increased surface area, and improved chemical stability, making them promising candidates for high-performance energy systems. Despite their potential, challenges, such as achieving scalable synthesis and uniform BN–GO dispersions and poor interface compatibility, have limited the widespread adoption of BN–GO hybrids. To address these limitations, this study is focused on the scalable synthesis of BN–GO composites *via* a liquid-phase exfoliation method with ultrasonication, followed by preparation of sodium thiosulfate (STS)-functionalized BN–GO composites (STBG), which exhibited high electrochemical properties suitable for energy storage. The structural identification was confirmed using FT-IR, Raman, XRD, and UV-vis spectroscopy. Thermal stability of the samples was assessed by TGA, while their morphological analysis was performed using HR-TEM, TEM, and SEM. Pristine BN showed negligible efficiency, whereas STS functionalization elevated the efficiency of STBN to 81.7%, while the incorporation of GO in STBG1 and STBG2 boosted their efficiency to 89.3% and 83.3%, respectively. STBG1 exhibited a nearly rectangular, symmetrical CV curve at various scan rates, demonstrating excellent capacitive behavior. Furthermore, it achieved the highest specific capacitance of 115.82 F g^{-1} at a current density of 1 A g^{-1}, together with a coulombic efficiency of 89.3%, indicating its superior charge transfer and minimal energy loss. Additionally, STBG1 retained 87.3% of its capacity, while STBG2 retained 81.7% even after 3000 charge/discharge cycles. These findings highlight that STBG1 is a promising composite with high capacitance, strong rate capability, and exceptional coulombic efficiency, making it a viable candidate for next-generation energy storage systems.

Received 14th November 2024
Accepted 8th January 2025

DOI: 10.1039/d4na00937a

rsc.li/nanoscale-advances

1 Introduction

In the era of growing energy demands, the sector of electrochemical energy storage is facing serious issues. Scientists and researchers are exploring various techniques and routes to overcome these concerns. The use of two-dimensional (2D) materials has opened new avenues to meet the demands of modern advancements.[1] 2D materials possess unique and distinct characteristics (thermal, optical, electronic, and magnetic), and are thus indulged in the production and design of various devices.[2] Most 2D materials enable electron mobility over their 2D plane surface (1–100 nm), thus enhancing their electromagnetic properties. The widely used 2D material is graphene. The sp^2 hybridized monolayer carbon atoms arranged in a hexagonal lattice structure in graphene endow it with peculiar properties, which has been widely used in many groundbreaking applications thus far. Graphene is also considered the thinnest material with an approximate thickness of about 0.335 nm.[3] Upon investigation, it was found that graphene-based composites show immense features, and thus could be incorporated in other 2D materials for future applications. Graphene oxide (GO) is an oxidized derivative of graphene *via* oxygen functional groups.[4] It is considered to be hydrophilic, and thus can be dispersed in aqueous solutions

[a]*Department of Physics, Noorul Islam Centre for Higher Education, Kumaracoil, Thuckalay, 629180, Tamilnadu, India. E-mail: bindhu.krishna80@gmail.com*
[b]*School of Chemical Engineering, Yeungnam University, 280 Daehak-Ro, Gyeongsan, 38541, Republic of Korea. E-mail: sshan@yu.ac.kr*
[c]*Department of Chemical Engineering, School of Mechanical, Chemical and Material Engineering, Adama Science and Technology University, Adama, P.O. Box-1888, Adama, Ethiopia. E-mail: ramesh.redrouthu@astu.edu.et*
[d]*Department of Chemistry, College of Science, King Saud University, Riyadh 11451, Saudi Arabia*
† Equally contributed.

unlike its hydrophobic precursor, graphene. However, GO exhibits some intrinsic limitations, including poor thermal stability, reduced active surface area, and aggregation tendency, which hinder its usage in some applications and necessitating further enhancements and functionalization. One promising approach to overcome these limitations is the incorporation of other 2D materials with superior properties. Hexagonal boron nitride (h-BN), with structural similarity to graphene, is known as "white graphene", which exhibits complementary properties such as excellent mechanical strength, thermo-chemical stability, and electrical insulation.[5–11] It was also noted that the bandgap of h-BN is about 6.07 eV.[12] Thus, these attributes make h-BN an ideal candidate to improve the performance of GO by preventing its restacking and enhancing the thermal management of the GO matrix, thus resulting in its application, particularly in energy storage and conversion applications. Alternatively, GO helps in the modification of the bandgap of h-BN, thus converting it from an insulator into a semiconductor/conductor. To fully exploit the synergistic benefits of h-BN, it is subjected to an exfoliation process, followed by proper functionalization. Subsequently, sodium thiosulphate (STS), $Na_2S_2O_3$, is used to functionalize the exfoliated BN, significantly increasing its properties. This functionalized BN is incorporated into GO to form STBN/GO composites, facilitating the formation of a robust and conductive network within the composite materials and introducing new active sites for electrochemical reactions. Functionalization not only prevents the agglomeration of BN/GO but also enhances the overall stability and conductivity of the composites, making them appropriate for energy-related applications.[13–17] The main problems encountered in energy storage applications are rapid charging and discharging cycles, achieving high surface area and cycling capacity, and poor long-term stability and performance of the device components, which limit traditional energy storage devices. For instance, lithium-ion batteries offer high energy density but suffer from limitations in their cycle life.[18] Alternatively, capacitors depict a high power density but fall short in terms of energy storage capacity.[19] Accordingly, STBN/GO composites offer advancements in this field. Additionally, the thermal stability and mechanical strength of BN contribute to the structural integrity of STBN/GO composites, making them desirable for high-temperature applications and flexible energy devices, addressing safety concerns associated with overheating.

In this present work, we report the novel synthesis of functionalized boron nitride/graphene oxide composites (see Scheme 1). Their synthesis involved simple dispersion and ultrasonication methods. The ultrasonication method aided in the dispersion of BN and GO, while prolonged stirring ensured thorough mixing of the materials. Hexagonal boron nitride was subjected to an exfoliation process, and then functionalized using sodium thiosulphate to form STBN. Subsequently, GO was dispersed in STBN to form STBN/GO composites. The structural, morphological and electrochemical studies of the samples were analyzed and the results are discussed.

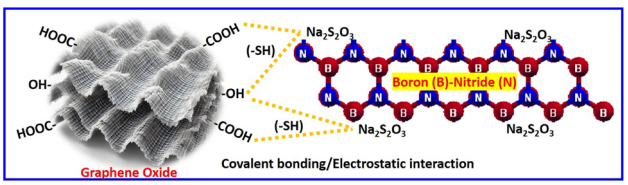

Scheme 1 Graphical representation of BN–GO nanocomposites.

2. Experimental section

2.1 Materials

Boron nitride (99%), graphene oxide, sodium thiosulphate, dimethyl formamide (DMF), and deionized water were purchased from Sigma Aldrich, USA (AR Grade).

2.2. Synthesis of STBN/GO composites

Liquid phase exfoliation was employed for the exfoliation process. Bulk BN was dispersed in DMF in a high-speed magnetic stirrer (500–800 rpm) for 35 min to pre-disperse the particles. Then, the dispersed BN was subjected to ultrasonication for 1 h to further prevent overheating and degradation. The ultrasonicated mixture was centrifuged at 5000 rpm to separate the exfoliated BN nanosheets. The supernatant was collected and dried in a vacuum oven at 60 °C for about 24 h. The dried samples were subjected to functionalization using sodium thiosulphate (STS). A 0.1 M STS solution was prepared in de-ionized water, ensuring it was freshly prepared to avoid degradation of the thiosulphate ions. The exfoliated BN was treated *via* the dropwise addition of STS (1 mL min^{-1}) under continuous stirring for 8 h to form STBN. The resulting mixture was centrifuged at 4000 rpm for 20 min to remove the unreacted STS. The washed sample was oven-dried at 60 °C for about 11 h to obtain STBN. GO was synthesized *via* the modified Hummers' method.[20] Different weight ratios of STBN to GO (1 : 2 and 1 : 3) were prepared (Table 1). These STBN/GO composites were stirred at 900 rpm for about 45 min to ensure homogeneity, followed by ultrasonication for 1 h to enhance the interaction and prevent agglomeration between STBN and GO. The resulting dispersion was centrifuged (5000 rpm, 30 min) and oven-dried (800 °C, 4 h) to promote its thermal stability and improve its interlayer bonding. These modifications ensured reproducibility and further paved the way for the optimization and mechanistic studies.

2.3 Material characterization

The structural studies and the crystalline nature of the prepared samples were analysed *via* X-ray diffraction (XRD)

Table 1 Weight ratios of STBN/GO composites

S. no	Ratio	GO (g)	STBN (g)	Sample code
1	1 : 2	0.3	0.6	STBG1
2	1 : 3	0.3	0.9	STBG1

characterization using an X-PERT-PRO X-ray diffractometer equipped with a CuKα source ($\lambda = 1.5218$ Å). A SHIMADZU IR Affinity-1 (FTIR spectrophotometer) was employed for Fourier transform infrared (FTIR) spectroscopy to determine the structural composition of the collected samples. Using a Carry 60 UV/visible spectrometer, the prepared samples were subjected to UV-visible absorption spectroscopy. A PerkinElmer Diamond device was utilized in a nitrogen-filled environment to carry out the thermogravimetric (TGA) analysis to study the composition and thermal stability of the samples.

2.4. Electrochemical characterization

The electrochemical characterizations were performed using an electrochemical workstation (SP-300 Biologic Instrument) with a three-electrode system utilizing 6 M aq. KOH electrolyte. Ag/AgCl was utilized as the reference electrode and platinum wires were used as the counter electrodes in this experimental setup. To create the functional electrode, each electrode was prepared by loading the surface of the current collector with the composite materials (STBG1 and STBG2). Cyclic voltammetry (CV) studies, galvanostatic charge–discharge (GCD) analysis, and cyclic tests studies were sequentially carried out for the samples. The CV profiles of the samples were recorded at different scan rates of 5 mV s^{-1}, 25 mV s^{-1}, 50 mV s^{-1}, 75 mV s^{-1}, and 100 mV s^{-1} in the potential window of 0 to 0.45 V. The GCD analysis was performed at different currents of 1 A g^{-1}, 2 A g^{-1}, 3 A g^{-1}, and 5 A g^{-1} in the same voltage window.

2.5. Electrochemical studies in a 3-electrode configuration system

In the energy studies, the 3-electrode configuration was mainly used to evaluate the electrochemical performance of the sample materials. The composition of the electrolyte and the working potential are the critical factors to consider in carrying out the electrochemical studies. Aqueous electrolytes are readily accessible, non-toxic, economical, and easy to handle. To carry out the electrochemical investigations of the synthesized sample and to analyse their charging and discharging, efficiency, and capacitive behaviours, a 6 M KOH (potassium hydroxide) aqueous electrolyte was used. Herein, aq. KOH dissociates into potassium (K^+) and hydroxide (OH^-) ions, facilitating ion conduction between the electrodes.[1] It also provides high ionic conductivity by reducing the internal resistance, a stable pH environment, minimizing the degradation of the electrode materials during the charging and discharging cycles, and also ensures efficient charge transfer.

3. Results and discussion

STBN/GO composites (STBG1 and STBG2) were synthesized. The powdered samples were subjected to X-ray diffraction to evaluate their crystal structure and purity. Fig. 1(a) shows a distinctive peak at the 2θ value of 26.61°, which aligns well with JCPDS card no. 34-0421 and corresponds to the (002) *hkl* plane of exfoliated BN.[21] Smaller peaks appeared at $2\theta = 20.3°$, 23.4°, and 26.6°, indicating the presence of graphene oxide.[22]

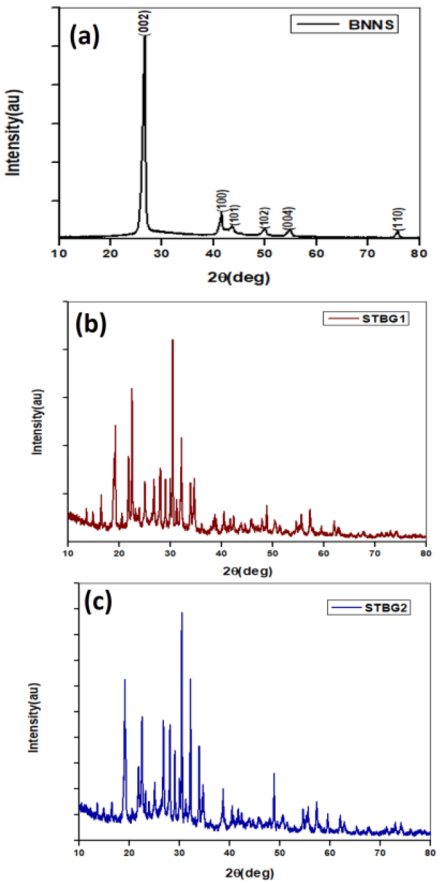

Fig. 1 XRD patterns of (a) exfoliated BN, (b) STBG1 and (c) STBG2.

Furthermore, less prominent peaks were observed at 54.96° and 41.48°. The X-ray diffraction pattern of STBG1 is shown in Fig. 1(b), where the signals at 19.08°, 22.59°, 26.67°, 30.61°, 33.20°, 34.14°, 34.75°, 38.92°, 49.68°, 55.66°, 62.16°, and 73.05° are identified as the typical peaks for STBG1. New peaks with high intensity appeared, which indicate the incorporation of STBN and GO. The peaks for STBG2 are illustrated in Fig. 1(c), which are located at 16.13°, 21.32°, 26.96°, 30.14°, 32.62°, 33.28°, 38.84°, 40.43°, 42.35°, 48.67°, 57.26°, and 62.03°. The peak at 26.96° indicates that the layered structure of GO was retained even after the addition of STBN. Higher crystallinity is indicated by the narrow-intense peaks in STBG1 and STBG2. An increase in peak intensity was obvious in STBG1 and STBG2 than in the exfoliated BN, implying the better dispersion of STBN in the GO matrix and better thermal and electrical properties.

The average crystallite size of STBN, STBG1 and STBG2 was calculated using the Scherrer equation, as follows:

$$D = K\lambda/\beta \cos\theta \quad (1)$$

It was noted that the size of the synthesized composites is in the nanoscale range. The corresponding strain was calculated. The dislocation density is a measure of dislocation/defects present in the material, which is related to its crystallite size and lattice strain (see Table 2).

Table 2 Crystallite size (D), lattice strain (ε) and dislocation density (ρ) of the synthesized composites

S. no	Sample	Crystallite size, D (Å)	Strain, ε (%)	Dislocation density (ρ)
1	STBN	309.4	0.370	1.04
2	STBG1	517.2	0.223	0.374
3	STBG2	487.6	0.317	0.421

The dislocation density (ρ) was calculated as follows:

$$\rho = 1/D^2 \quad (2)$$

where 'D' is the crystalline size.

STBG1 with the largest crystalline size [517.2 Å] showed the lowest dislocation density. STBG2 also exhibited good crystallinity but it was slightly inferior to that of STBG1. Functionalization and introduction of GO into BN lattice induced strain, which created microstructural distortion. In the case of STBG1 and STBG2, the strain decreased compared to that of STBN, indicating their enhanced structural stability due to the incorporation of GO.

The FTIR analysis of STBG1 and STBG2 within the spectral range of 500 to 4000 cm^{-1} is shown in Fig. 2. The STBN/GO composites reveal distinct peaks indicating the presence of various functional groups and bonding interactions. The peaks in the spectrum of exfoliated BN are located at 813.15 cm^{-1} and 1384.70 cm^{-1} (see Fig. 2(a)). STBG1 revealed FTIR peaks at 607 cm^{-1}, 1015 cm^{-1}, 1243 cm^{-1}, 1252 cm^{-1}, 1393 cm^{-1}, 1606 cm^{-1}, and 2368 cm^{-1} (see Fig. 2(b)). The peak at 607 cm^{-1} is due to the bending vibrations induced in BN in STBG1 upon its functionalization using sodium thiosulphate. The peak at 1393 cm^{-1} also confirms the presence of BN. The FTIR spectrum of STBG2 exhibits characteristic peaks at 599 cm^{-1}, 1007 cm^{-1}, 1109 cm^{-1}, 1235 cm^{-1}, 1385 cm^{-1}, 2352 cm^{-1}, and 3477 cm^{-1} (Fig. 2(c)). The presence of oxygenated functional groups from GO is indicated by the peaks at 1015 cm^{-1} and 1007 cm^{-1} in both STBG1 and STBG2. An intense V-shaped peak is obtained in the spectrum of STBG2 compared to that of STBG1, which exhibits the B–O stretching vibrations in the composite. The broad U-shaped peak at 3500 cm^{-1} and 3477 cm^{-1} represents the presence of O–H vibrations in STBG1 and STBG2, respectively. The variations in the peak positions in the composite materials are because of the difference in their degree of functionalization, ratio of samples mixed, and interaction between the individual components, STBN and GO.

The UV-visible analysis provides the adsorption peaks exhibited by the synthesized composites, thus delivering insights into their electronic transitions, as depicted in Fig. 3.

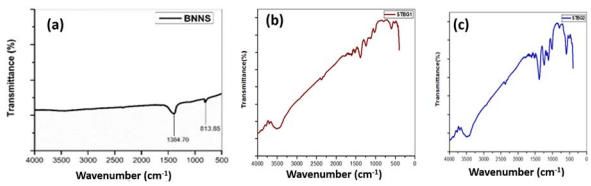

Fig. 2 FTIR spectra of (a) exfoliated BN, (b) STBG1 and (c) STBG2.

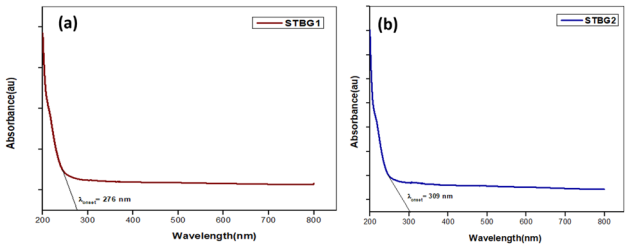

Fig. 3 UV-visible analysis of (a) STBG1 and (b) STBG2.

The UV-visible spectra of exfoliated BN and graphene oxide show distinctive peaks at 215 nm and 226 nm, respectively.[23,24] The positioning of the peak as well as its intensity ensures the electronic structure of a material. The energy–wavelength equation is identified as Energy (eV) = 1240/λ_{onset} (nm), where λ_{onset} is the wavelength. Table 3 presents the calculated energy (eV) of the composite materials.

In Fig. 3(a), STBG1 exhibits a peak at 276 nm, indicating that the electronic structure of the STBN/GO composite differs from that of the exfoliated BNNS. The coupling between STBN and GO resulted in the formation of a hybrid electronic structure with extended π-conjugation across the interface. The greater incorporation of STBN enhanced the overall conjugation within the composite material, further decreasing the energy bandgap. The interaction between STBN and GO modified the density of states near the valence band and conduction band of the composite, resulting a shift in their UV visible spectral analysis. The formation of a new bond between STBN and GO resulted in the hybridization of the orbitals, thus tuning the energy levels and band gaps. The physical mechanism involves a reduction in the energy gap due to the hybridization of the electronic state between GO and STBN, with an enhancement in the delocalization of π-electrons. The interactions between STBN and GO induced changes in the energy levels of the composite material, thus initiating a shift in the adsorption peak. The peak at 309 nm corresponds to the STBG2 composite (Fig. 3(b)). The increase in STBN content in the STBG2 composite resulted in an increase in the overall conjugation in the composite. Greater conjugation resulted in a decrease in the energy gap value.

The theoretical analysis of the modification mechanism of sodium thiosulphate-functionalized boron nitride (STBN) and GO composites is pivotal to support the experimental findings, particularly regarding their electronic properties such as bandgap reduction. Density functional theory (DFT) and quantum mechanical calculations involve computational calculations to identify the electronic interactions as well as densities in predicting the properties of a material. The

Table 3 Energy calculations based on λ_{onset} values of STBN/GO composites

S. no	Sample code	λ_{onset} (nm)	Energy (eV)
1	Exfoliated BN	204	6.07 (ref. 25)
2	STBG1	276	4.49
3	STBG2	309	4.01

mechanical properties of the sodium thiosulphate-functionalized boron nitride-based graphene oxide composites (STBG1 and STBG2) were significantly improved by their structural interactions. The DFT calculations revealed the integration of these two materials, leading to improved hardness and tensile strength, which are crucial in developing robust materials for engineering applications.[26] Adjusting the composition ratios of BN and GO also tunes their electronic properties, including bandgap.[27] It is also evident from the DFT calculations that the electronic bandgap of BN was reduced from 5.94 eV to 11.61 eV with the incorporation of dopants and graphene monolayers.[28] The bandgap reduction in STBG1 and STBG2 is correlated with the theoretical findings. The UV-visible analysis showed a narrowing in their bandgap. The theoretical models also predicted this behavior by simulating the interface states and hybridized electronic structures. Therefore, the theoretical analysis initiates a framework for explaining the experimental results of bandgap reduction in the BN–GO composites, supporting our experimental work.

TGA analysis was employed to investigate the change in the mass of the samples with temperature. Fig. 4 indicates the occurrence of phase transitions within the samples with a change in temperature in a controlled nitrogen atmosphere. Fig. 4(a–c) present the TGA curves for BNNS, STBG1, and STBG2, respectively. The temperature at which exfoliated BN begins to degrade was estimated to be at 203.5 °C, with a total weight loss of 0.5% recorded. The onset degradation temperature of STBG1 is located at 165.3 °C in Fig. 4(b). In addition, there is an immediate mass loss of about 2.35%. The elimination of volatile components or surface species from the boron nitride-graphene oxide composite as the temperature increased is reflected in the initial mass loss measured during the TGA analysis. The reduction in mass was determined to be 18.88% and 8.56% before the stable plateau area. The thermal breakdown patterns of graphene oxide and boron nitride differ. Thus, the combined breakdown of the two components is responsible for the mass loss evident in the composite. Functional groups containing oxygen, such as epoxides and carbonyls, are bound to the carbon structure of graphene oxide. These functional groups are prone to breaking down at high temperatures during the TGA analysis. There is a significant mass loss in STBG1 when these components split apart and are desorbed as gases. According to Fig. 4(c), STBG2 displays the onset degradation temperature at 150.8 °C with mass losses of 3.35%, 20.21%, and 7.35%, respectively. The initial weight loss is explained by the high-temperature vaporization of the adsorbed water molecules on the STBG2 surface. In addition, the TGA investigation implies that in comparison to boron nitride and graphene oxide, this composite material is more susceptible to thermal degradation at lower temperatures.

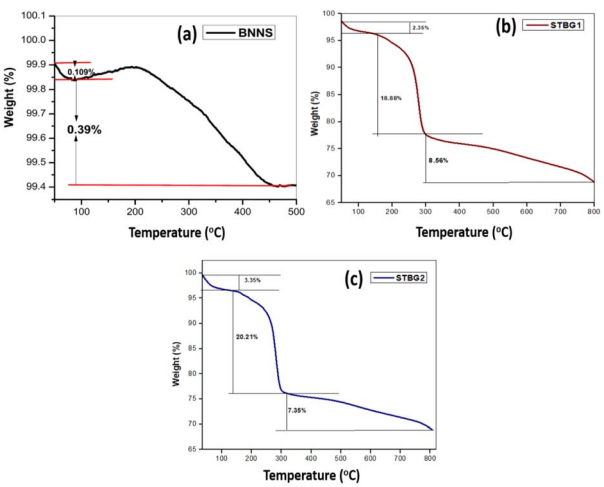

Fig. 4 TGA analysis of (a) exfoliated BN, (b) STBG1 and (c) STBG2.

The cyclic voltammetry (CV) analysis of STBN, STBG1, and STBG2 was tested in a 3-electrode configuration at different scan rates (5 mV s^{-1}, 25 mV s^{-1}, 50 mV s^{-1}, 75 mV s^{-1}, and 100 mV s^{-1}) in the potential window of 0 to 0.45 V, as presented in Fig. 5. Fig. 5(a) illustrates the CV curve of STBN at different scan rates. The CV curve of STBN at lower scan rates indicates capacitive behavior similar to the electric double-layer capacitance (EDLC) nature. At higher scan rates, the CV curves became more distorted, resulting in large current responses, which increased the peak current density, introducing resistive losses and reduced capacitance.

The mechanism explaining the redox process at STBN is as follows:

• Boron nitride is exfoliated (e-BN) and functionalized using sodium thiosulphate. The thiosulphate ions from the solution adsorb on the surface of e-BN. The thiosulphate peaks undergo oxidation at the anodic peaks to form sulfate ions, releasing water and electrons.

$$S_2O_3^{2-} + 5OH^- \rightarrow 2SO_4^{2-} + 3H_2O + 4e^- \quad (3)$$

• The cathodic reactions involve the reduction of hydroxide ions to water, producing electrons. The water molecules are reduced to form hydrogen gas and hydroxide ions.

$$2H_2O + 2e^- \rightarrow 2OH^- + H_{2(g)} \quad (4)$$

These reactions indicate that the redox process is reversible with thiosulphate and sulfate ions interconverting in the potential range of 0 to 0.45 V. The CV curves of STBG1 depict a quasi-rectangular-shaped curve at lower scan rates, depicting capacitive behavior, which is characteristic of materials utilized in supercapacitors (see Fig. 5(b)). The STBG1 composite exhibits EDLC behavior as its primary charge storage mechanism.[29–35] The symmetry of the curves for STBG1 between the positive and negative sweeps specifies its good reversibility in the charging–discharging process. At a scan rate of 5 mV s^{-1}, the CV curves of STBG1 are more rectangular, as the ions form a stable double layer at the electrode–electrolyte interface, suggesting efficient charge storage with minimal resistive losses. STBG1 exhibited excellent capacitive behavior even at a high scan rate. The current density increased with the scan rate, and thus STBG1 can handle higher currents. The presence of GO in STBG1 enhanced its electrical conductivity and overall capacitance, facilitating further electron transfer. Fig. 5(c) illustrates the CV curves of the STBG2 composite. At a lower scan rate, the 5 mV

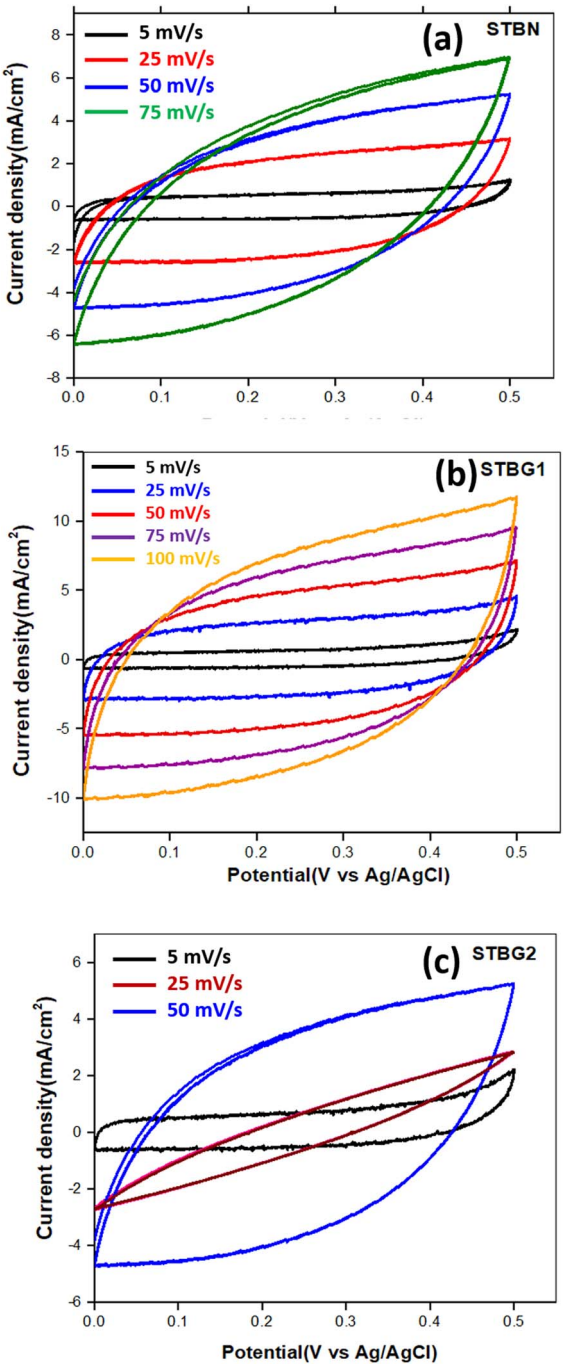

Fig. 5 Electrochemical analysis of the electrode materials in 6 M aq. KOH in a 3-electrode system. Voltammograms of (a) STBN, (b) STBG1, and (c) STBG2 at varying scanning rates.

s^{-1}, STBG2 composite exhibited good capacitive behavior. At a higher scan rate of 75 mV s^{-1}, the CV curves became more distorted with a substantial increase in the current density and more prominent skewness. The increase in STBN content in STBG2 compared to that of STBG1 introduced more resistive elements, increased number of active sites, and potential aggregation, particularly at higher scan rates. The CV curves of STBG1 cover the largest area among the samples, indicating high capacitive behavior.

The GCD test of STBN, STBG1, and STBG2 was performed at current densities of 1 A g^{-1}, 2 A g^{-1}, 3 A g^{-1}, and 5 A g^{-1} in the potential window of 0 to 0.45 V. in an aq. KOH electrolyte in a 3-electrode system, as illustrated in Fig. 6. The symmetrical shape of the charge–discharge curves and the triangular features indicate strong electrochemical capacity, sufficient reversibility, and a significant contribution to EDLC nature. The main metric used to evaluate the performance of an electrode is specific capacitance (CSC), which quantifies the ability of an electrode to store and deliver electric charges and is proportional to the discharge time obtained from the GCD curves. The specific capacitance is mathematically expressed using the following equation:

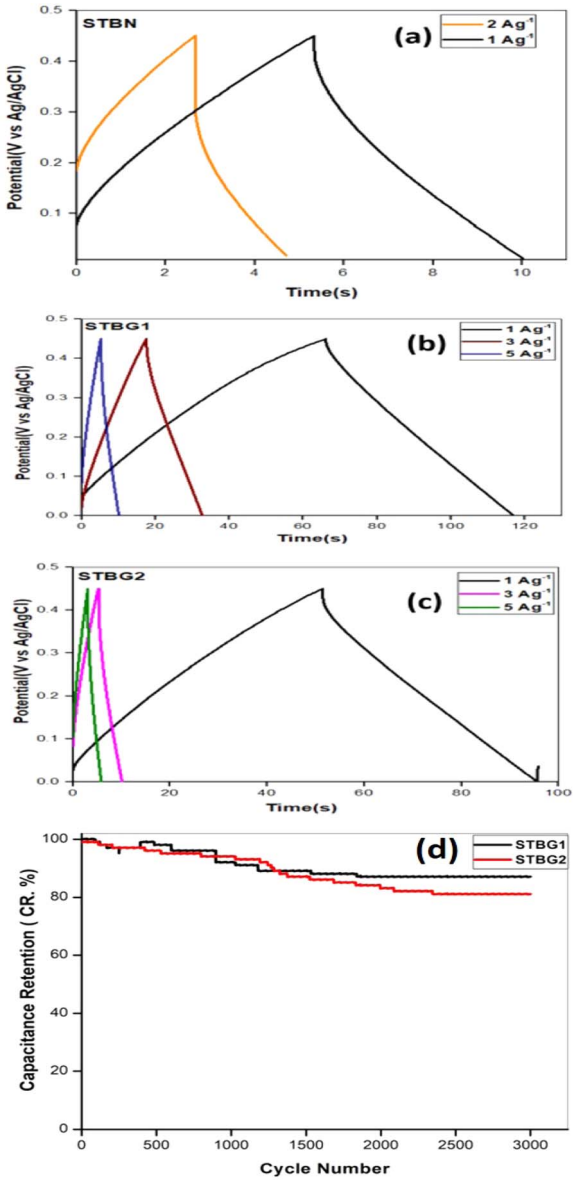

Fig. 6 Galvanostatic charge–discharge (GCD) curves of (a) STBN, (b) STBG1, and (c) STBG2 represented at different current densities. (d) Cyclic stability (capacitance retention *vs.* cycle number) of STBG1 and STBG2 composites.

$$C_{SC} = \frac{i \times \Delta t}{m \times \Delta V} \quad (5)$$

where C_{SC} is the specific capacitance expressed in F g^{-1}, i is the discharge current (A), Δt is the discharge time (s), m is the mass of the electrode material (g) and ΔV is the potential difference (V). It is also evident that a higher CSC value indicates a greater ability to deliver and store charge for a given mass of electrode material.

The CSC of STBN, STBG1, and STBG2 at a current density of 1 A g^{-1} was calculated to be 10.62 F g^{-1}, 115.82 F g^{-1}, and 99.15 F g^{-1}, respectively. Compared to STBN, the CSC value of STBG1 and STBG2 increased due to the presence of graphene oxide (GO) in them. GO provides numerous active sites in the STBG1 and STBG2 composites for electrochemical reactions due to its large surface area. STBG1 exhibited a greater specific capacitance given that it is comprised of a lower STBN ratio compared with STBG2. The improved conductivity in STBG1 and STBG2 reduced the internal resistance in these composites, allowing faster charging–discharging rates and higher CSC values than STBN. The GCD analysis of the samples matches well with the CV analysis. The CSC of STBN at a current density of 2 A g^{-1} is 8.93 F g^{-1} (see Fig. 6(a)). The CSC value decreased with an increase in current density. The limited surface area in STBN for ion adsorption and charge storage restricted its overall capacitance.

The CSC of STBG1 at current densities of 3 A g^{-1} and 5 A g^{-1} was 109.06 F g^{-1} and 57 F g^{-1}, respectively (Fig. 6(b)). Fig. 6(c) indicates that the specific capacitance of STBG2 at the above-mentioned current densities is 31.46 F g^{-1} and 28.44 F g^{-1}, respectively. The electrochemical performance of the samples was evaluated using coulombic efficiency (CE), which represents the ratio of discharge time to charging time in a charge–discharge cycle. The efficiency of pristine boron nitride is negligibly small. Upon functionalizing BN using sodium thiosulphate, STBN exhibited an efficiency of 81.7%, given that thiosulphate groups introduce conductive groups on the surface of BN, thus improving its conductivity. Accordingly, STBG1 and STBG2 samples also exhibited a high efficiency of about 89.3% and 83.3% due to the addition of GO. The rate capability of 0.492 for STBG1 revealed that it retained a significant portion of its specific capacitance at high current densities. STBG2 showed a lower rate capability of 0.28, which ensures that its performance is more sensitive to high current densities.

Cyclic stability is a crucial parameter to investigate the long-term performance of battery/supercapacitor applications.[36] A higher capacitance retention value denotes the better stability of the material, and therefore it can withstand multiple charge–discharge cycles with a minimum loss in its capacity. The electrochemical performance was determined for the STBG1 and STBG2 composites galvanostatically charged and discharged for about 3000 cycles. Fig. 6(d) indicates the cyclic performance and stability of the STBG1 and STBG2 composites, which exhibited a gradual decrease in capacitance retention with an increase in the number of cycles. STBG1 consistently indicated a higher capacitance retention of about 87.3%. The capacitance retention of 81.7% was observed for the STBG2 composite in the tested cycle range. The superior performance of STBG1 is due to its structural stability, electrolyte compatibility and enhanced charge transfer kinetics. The incorporation of GO in STBN improved its surface area and introduces more active sites. This ensured faster charge transfer and lowered the resistance during cycling, contributing high coulombic efficiency, as observed in STBG1. The strong interfacial bonding in STBG1 minimized the material degradation during repeated cycling, enhancing its capacity retention value compared to that of STBG2.

Scanning electron microscopy (SEM) is an indispensable tool in materials science, offering insights into the surface morphology and microstructural characteristics of materials. The SEM image of sodium thiosulphate-functionalized BN (STBN) is presented in Fig. 7(a). The SEM images revealed a heterogeneous distribution of STBN with varying sizes and

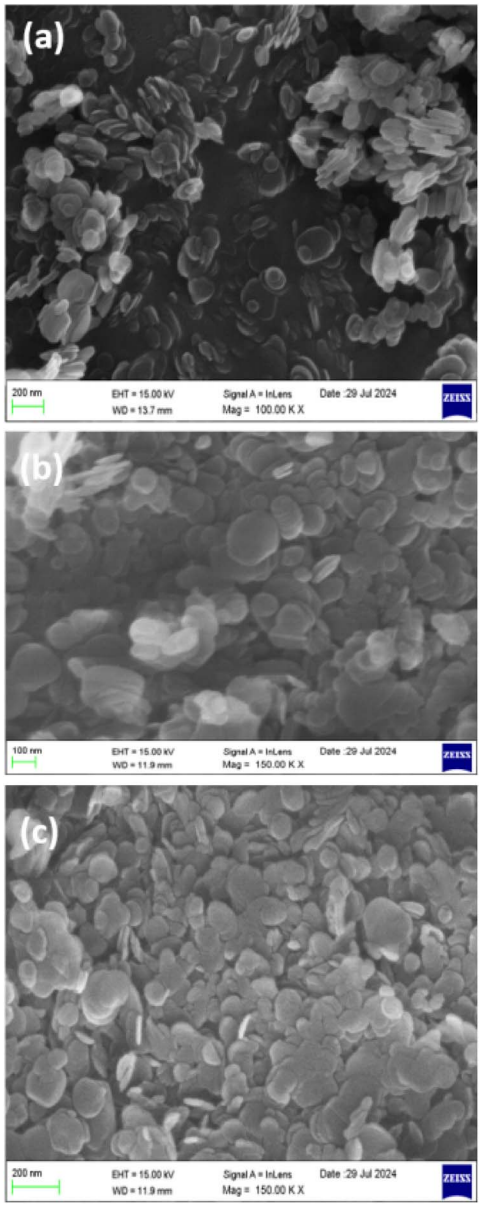

Fig. 7 SEM images of (a) STBN, (b) STBG1 and (c) STBG2 composite.

shapes. The SEM images of the exfoliated BN indicate the presence of characteristic sheet-like structures. STBN depicted oval-shaped flakes that are crumbled and folded, indicating layered structures. Some regions display multiple flakes clustered together and are the key evidence for agglomeration. Agglomeration is visible at distinct places due to the van der Waals forces between the BN layers. The scale bar (200 nm) portrays that the lateral dimensions of the individual nanosheets in the range of approximately 100 nm to 300 nm. The SEM images of the composite materials comprised of STBN/graphene oxide (GO), STBG1 and STBG2, are depicted in Fig. 7(b and c), respectively. The sheet-like wrinkled structures with a relatively smooth surface in STBG1 represent the presence of GO in the composite. A uniform distribution of STBG1 regions with higher concentrations of each component (STBN and GO) overlaps and intersects with each other. Noticeable aggregates are seen in certain domains, where STBN flakes and GO clustered together, where the presence of GO provides an additional surface area to the composites and facilitates better interfacial bonding. STBN flakes are discernible and uniformly dispersed in the STBG2 composite. The larger continuous region reveals the presence of GO sheets, which support and blend with the STBN structure for the successful incorporation and formation of the STBG2 composites. Functionalizing BN improved the interaction between BN and GO. Closely packed aggregates were obvious in the SEM analysis. It is also noticeable that the higher concentration of STBN in GO induced particle agglomeration given that sodium thiosulfate (STS) is hydrophilic, which is visible in the STBG2 composite when compared to STBG1.

A novel approach to improve the electrochemical properties of STBN/GO composites is using STS as a functionalizing agent. The ultrasonication process disrupts the van der Waals forces between the boron nitride layers, further resulting in the exfoliation of BN sheets. The ultrasonication step also increased the surface area of BN and generated active sites on the surface of the nanosheets. It is also noted that sodium thiosulphate is a strong nucleophile, and thus it reacted with the surface defects/active sites as well the functional groups on BN nanosheets. The thiosulphate in STS formed covalent bonds with the metal ions present in the structure of BN. STS also improved the dispersibility of BN in aqueous media and facilitated the formation of strong interfacial bonds with GO. The introduction of STS resulted in a change in the conductivity of the composite by providing additional charge carriers. Thus, the functionalized BN nanosheets facilitated efficient charge transfer, thus improving the electrochemical performances. The combination of conductive graphene oxide and STS-functionalized BN also created a highly conductive network, further improving the overall electrochemical performance of the composite.

Raman analysis provides valuable insights into the structural and compositional characteristics of materials. The Raman spectra of STBN, STBG1 and STBG2 are presented in Fig. 8(a–c), respectively. The STBN sample exhibited Raman peaks at 274 cm^{-1}, 656 cm^{-1}, 829 cm^{-1} and 1012 cm^{-1}. The Raman spectrum of STBN showed the characteristics peaks of

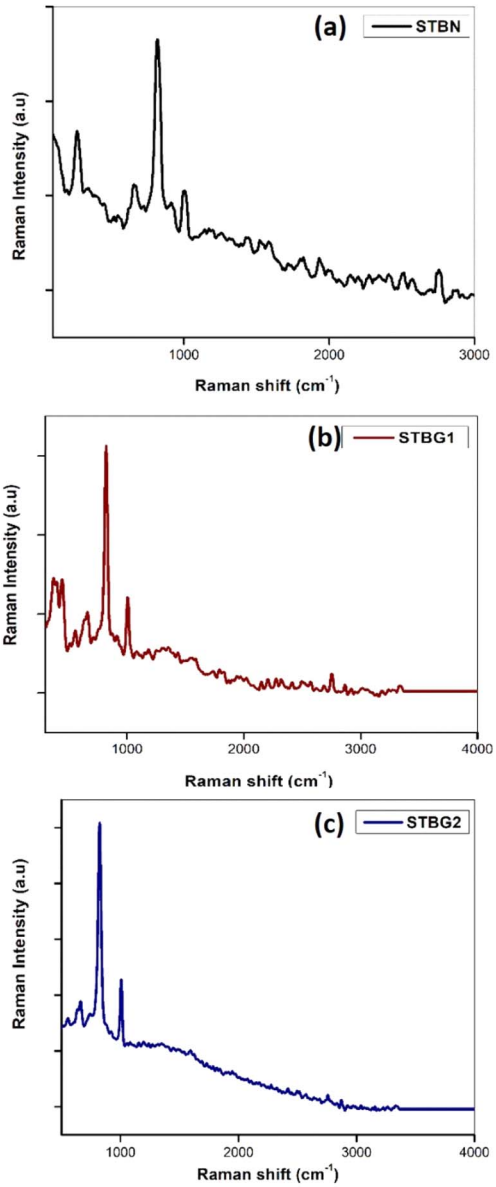

Fig. 8 Raman analysis of (a) STBN, (b) STBG1 and (c) STBG2 composites.

BN, confirming its presence in the sample. The peak at 274 cm^{-1} corresponds to the symmetric stretching of the BN bonds, while the sharp and intense peak at 829 cm^{-1} represents the S–S stretching mode of the STS, which introduced new functional groups, altering the vibrational modes of the existing groups and leading to shifts in its Raman peaks.

STBG1 displays the Raman peaks at 434 cm^{-1}, 669 cm^{-1}, 832 cm^{-1} and 1016 cm^{-1}, while STBG2 exhibits peaks at 662 cm^{-1}, 836 cm^{-1}, and 1003 cm^{-1}. Additionally, both STBG1 and STBG2 show a D band at 1355 cm^{-1} and G band at 1612 cm^{-1}, confirming the presence of graphene in the composites. The appearance of new peaks in STBG1 and STBG2 indicates bending vibrational modes, resulting from the interaction between GO and STBN. The shifts in Raman peaks for STBG1 and STBG2 compared to STBN suggest changes in

bonding and strain caused by STS functionalization and the incorporation of GO. The addition of GO induced significant structural modifications in STBG1 and STBG2, as evidenced by the new peaks and noticeable shifts in its Raman spectrum. These shifts indicate strong interactions between STBN and GO, leading to charge transfer and vibrational and electronics properties of STBG1 and STBG2, demonstrating the synergy between STBN and GO in the composites.

The high-resolution transmission electron microscopy (HR-TEM) images of STBN, STBG1 and STBG2 are denoted in Fig. 9(a–c), respectively. The HR-TEM image of STBN reveals a predominant structure with regions of poorly defined lattice fringes. In contrast to STBN, the HR-TEM images of STBG1 and STBG2 reveal a distinct flower-like structures dispersed across the GO matrix, formed by the aggregation of STBN and GO, resulting in a greater surface area and increased active sites for potential reactions and catalytic activities. Clear lattice fringes are visible particularly in regions adjacent to the STBN/GO interfaces. The wrinkled structure of GO is visible and helps to accommodate STBN. The STBG1 and STBG2 composites display well defined lattice fringes, initiating the preservation of the crystallinity of BN with good bonding in the GO matrix (see Fig. 9(b and c)). The interplanar spacing of STBN, STBG1 and STBG2 was determined to be 3.46 Å, 3.28 Å and 3.43 Å, respectively. The relatively lower amount of STBN in STBG1 compared to STBG2 resulted in superior characteristics in terms of functionality. The transmission electron microscopy (TEM) images of STBN, STBG1 and STBG2 highlight the structural and morphological variations between STBN and its composites with graphene oxide (STBG1 and STBG2), respectively. The images were captured at a uniform scale of 20 nm, allowing a comparative evaluation. Fig. 9(d) exhibits the TEM image of STBN, revealing a distinctly layered dense morphology and a uniform distribution of layers. The successful functionalization with sodium thiosulphate enhanced the dispersibility of BN. In STBG1, the STBN particles appears to be relatively small and uniformly distributed with GO, indicating good interfacial interaction between STBN and GO (see Fig. 9(e)). Fig. 9(f) illustrates the TEM image of STBG2, possessing a higher density of STBN particles than STBG1. The increase in STBN content in STBG2 led to aggregation with visible clusters. These agglomerates indicate the reduced dispersion of STBN at a higher loading, hindering the overall integration of the composite.

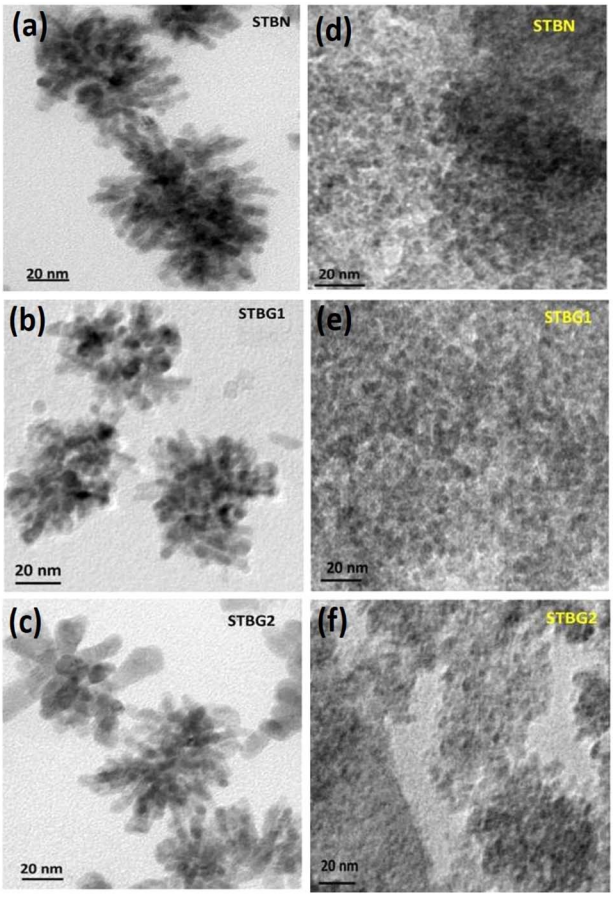

Fig. 9 HR-TEM images of (a) STBN, (b) STBG1 and (c) STBG2. TEM images of (d) STBN, (e) STBG1, and (f) STBG2.

4. Conclusion

The incorporation of GO in the functionalized STBN matrix significantly increased the electrochemical characteristics of the composite. XRD analysis revealed the formation of exfoliated boron nitride, where the newer peaks in the XRD patterns of STBG1 and STBG2 signify the successful incorporation and formation of STBN/GO composites. Also, the increase in the peak intensity in the patterns of STBG1 and STBG2 confirmed that the crystalline nature of BNNS was retained after the formation of the BN–GO composites, which resulted in better conductivity. Sodium thiosulphate functionalization also enhanced the properties of both materials (BN and GO) by providing chemical stability. According to the UV analysis, the corresponding energy bandgap values of STBG1 and STBG2 were determined to be 4.49 eV and 4.01 eV, respectively. The incorporation of graphene oxide into the boron nitride matrix introduced defects, edges, and functional groups, which could induce localized states within the bandgap. These defects and interfaces could create additional energy levels within the bandgap, reducing its effective width. As a result, the bandgap of the composite materials became narrower compared to pristine boron nitride, whose bandgap is about 6.07 eV. There was an improvement in the efficiency of the STBG1 and STBG2 composites in the charge–discharge cycles. The CV curves of STBG1 remained more rectangular and symmetrical at different scan rates, indicating its superior capacitive nature to that of STBN. STBG1 exhibited the highest capacitance of 115.82 F g^{-1} at a current density of 1 A g^{-1} this is due to the optimal ratio of STBN to GO, which facilitated efficient charge storage, and also reduced the internal resistance. STBG2 also showed an improved capacitance than STBN, though slightly lower than STBG1, which is likely due to the presence of a higher STBN content, introducing more resistive elements. STBN showed a lower capacitance given that it was less conductive and had a reduced active surface area. STBG1 and STBG2 exhibited a coulombic efficiency of about 89.3% and 83.3%, respectively, due to the incorporation of GO, ensuring better charge transfer

and minimal energy loss. The capacity retention of STBG1 was 87.3% and STBG2 was 81.7% after charging and discharging for about 3000 cycles. STBG1, in particular, stands as a promising composite with high specific capacitance and capacity retention values, good rate capability, and excellent coulombic efficiency. Thus, functionalizing BN with sodium thiosulphate and incorporating of GO is considered an effective strategy for enhancing the electrochemical performance of pristine boron nitride. This composite offers promising application in many energy storage devices, particularly supercapacitors.

Data availability

The data that support the findings of this study are available from the corresponding author upon reasonable request.

Conflicts of interest

All the authors approve that there are no conflicts of interest to declare.

Acknowledgements

The authors would like to extend their sincere gratitude to Noorul Islam Centre for Higher Education, Tamil Nadu, and the Department of Science and Technology (DST), New Delhi, for assisting in carrying out this research work. This project was supported by Researchers Supporting Project number (RSP2025R238), King Saud University, Riyadh, Saudi Arabia. This project was also supported by the National research foundation of Korea (NRF) (Grant no.: 2020R1A6A1A03044512).

References

1 M. M. Uddin, M. H. Kabir, M. A. Ali, M. M. Hossain, M. U. Khandaker, S. Mandal and D. Jana, Graphene-like emerging 2D materials: recent progress, challenges and future outlook, *RSC Adv.*, 2023, **13**(47), 33336–33375.
2 S. O. A. Ahmad, A. Ashfaq, M. U. Akbar, M. Ikram, K. Khan, F. Wang and A. Mahmood, Application of two-dimensional materials in perovskite solar cells: recent progress, challenges, and prospective solutions, *J. Mater. Chem. C*, 2021, **9**(40), 14065–14092.
3 V. Kumar, A. Kumar, D. J. Lee and S. S. Park, Estimation of number of graphene layers using different methods: a focused review, *Materials*, 2021, **14**(16), 4590.
4 I. Ferrari, A. Motta, R. Zanoni, F. A. Scaramuzzo, F. Amato, E. A. Dalchiele and A. G. Marrani, Understanding the nature of graphene oxide functional groups by modulation of the electrochemical reduction: A combined experimental and theoretical approach, *Carbon*, 2023, **203**, 29–38.
5 M. Zahoor, S. Khan, P. M. Ismail, L. Qiao, M. Haneef, J. Akbar and S. Ali, Introduction to hexagonal boron nitrides: history, classification, structure, fundamental properties, challenges, and future perspective, ,in *Hexagonal Boron Nitride*, Elsevier, 2024, pp. 3–28.
6 A. E. Naclerio and P. R. Kidambi, A review of scalable hexagonal boron nitride (h-BN) synthesis for present and future applications, *Adv. Mater.*, 2023, **35**(6), 2207374.
7 J. Wang, F. Ma, W. Liang and M. Sun, Electrical properties and applications of graphene, hexagonal boron nitride (h-BN), and graphene/h-BN heterostructures, *Mater. Today Phys.*, 2017, **2**, 6–34.
8 X. Wang, M. Hossain, Z. Wei and L. Xie, Growth of two-dimensional materials on hexagonal boron nitride (h-BN), *Nanotechnology*, 2018, **30**(3), 034003.
9 N. Kostoglou, K. Polychronopoulou and C. Rebholz, Thermal and chemical stability of hexagonal boron nitride (h-BN) nanoplatelets, *Vacuum*, 2015, **112**, 42–45.
10 X. Wang, M. Hossain, Z. Wei and L. Xie, Growth of two-dimensional materials on hexagonal boron nitride (h-BN), *Nanotechnology*, 2018, **30**(3), 034003.
11 S. Roy, X. Zhang, A. B. Puthirath, A. Meiyazhagan, S. Bhattacharyya, M. M. Rahman and P. M. Ajayan, Structure, properties and applications of two-dimensional hexagonal boron nitride, *Adv. Mater.*, 2021, **33**(44), 2101589.
12 J. Hassan, S. Naz, A. Haider, A. Raza, A. Ul-Hamid, U. Qumar and M. Ikram, h-BN nanosheets doped with transition metals for environmental remediation; a DFT approach and molecular docking analysis, *Mater. Sci. Eng., B*, 2021, **272**, 115365.
13 J. Wang, F. Ma and M. Sun, Graphene, hexagonal boron nitride, and their heterostructures: properties and applications, *RSC Adv.*, 2017, **7**(27), 16801–16822.
14 L. Ci, L. Song, C. Jin, D. Jariwala, D. Wu, Y. Li and P. M. Ajayan, Atomic layers of hybridized boron nitride and graphene domains, *Nat. Mater.*, 2010, **9**(5), 430–435.
15 C. R. Dean, A. F. Young, I. Meric, C. Lee, L. Wang, S. Sorgenfrei and J. Hone, Boron nitride substrates for high-quality graphene electronics, *Nat. Nanotechnol.*, 2010, **5**(10), 722–726.
16 M. Yankowitz, J. Xue and B. J. LeRoy, Graphene on hexagonal boron nitride, *J. Phys.: Condens. Matter*, 2014, **26**(30), 303201.
17 J. Wang, F. Ma, W. Liang and M. Sun, Electrical properties and applications of graphene, hexagonal boron nitride (h-BN), and graphene/h-BN heterostructures, *Mater. Today Phys.*, 2017, **2**, 6–34.
18 X. Shen, H. Liu, X. B. Cheng, C. Yan and J. Q. Huang, Beyond lithium ion batteries: Higher energy density battery systems based on lithium metal anodes, *Energy Storage Mater.*, 2018, **12**, 161–175.
19 R. T. Yadlapalli, R. R. Alla, R. Kandipati and A. Kotapati, Super capacitors for energy storage: Progress, applications and challenges, *J. Energy Storage*, 2022, **49**, 104194.
20 B. Jebanisha, V. M. Devi, J. Varghese and N. R. Aswathy, Magnetic and dielectric characteristics of rGO modified BFO nanoparticles produced using sol-gel *via* auto-combustion method, *Ceram. Int.*, 2024, **50**(19), 36955–36963.
21 R. M. Nair, B. Bindhu and S. A. Thomas, Hydroxylation of boron nitride nanosheets, *AIP Conf. Proc.*, 2020, **2265**, 030695.
22 R. Siburian, H. Sihotang, S. L. Raja, M. Supeno and C. Simanjuntak, New route to synthesize of graphene nano sheets, *Orient. J. Chem.*, 2018, **34**(1), 182.

23 P. Kumbhakar, A. K. Kole, C. S. Tiwary, S. Biswas, S. Vinod, J. Taha-Tijerina and P. M. Ajayan, Nonlinear optical properties and temperature-dependent uv–vis absorption and photoluminescence emission in 2d hexagonal boron nitride nanosheets, *Adv. Opt. Mater.*, 2015, **3**(6), 828–835.
24 T. F. Emiru and D. W. Ayele, Controlled synthesis, characterization and reduction of graphene oxide: A convenient method for large scale production, *Egypt. J. Basic Appl. Sci.*, 2017, **4**(1), 74–79.
25 Z. Zhao, Z. Yang, Y. Wen and Y. Wang, Facile synthesis and characterization of hexagonal boron nitride nanoplates by two-step route, *J. Am. Ceram. Soc.*, 2011, **94**(12), 4496–4501.
26 G. Casiano-Jiménez, C. Ortega-López, J. A. Rodríguez-Martínez, M. G. Moreno-Armenta and M. J. Espitia-Rico, Electronic structure of graphene on the hexagonal boron nitride surface: a density functional theory study, *Coatings*, 2022, **12**(2), 237.
27 W. Zhan, H. Wang, J. Gao, X. Tang, X. Zhu, Y. Xiao and H. Yin, Hexagonal Boron Nitride/Reduced Graphene Oxide Heterostructures as Promising Metal-Free Electrocatalysts for Oxygen Evolution Reaction Driven by Boron Radicals, *Small Struct.*, 2023, **4**(11), 2300167.
28 E. M. O'Sullivan, N. Grobert and M. Swart, Density Functional Theory Investigation of 2D Phase Separated Graphene/Hexagonal Boron Nitride Monolayers; Band Gap, Band Edge Positions, and Photo Activity, *J. Phys. Chem. C*, 2024, **129**(1), 638–647.
29 K. Ashok Kumar, A. Pandurangan, S. Arumugam and M. Sathiskumar, Effect of bi-functional hierarchical flower-like CoS nanostructure on its interfacial charge transport kinetics, magnetic and electrochemical behaviors for supercapacitor and DSSC applications, *Sci. Rep.*, 2019, **9**(1), 1228.
30 M. M. Momeni, H. M. Aydisheh, B. K. Lee, H. Farrokhpour and M. Najafi, Preparation of photo-rechargeable asymmetric supercapacitors using S, W-codoped titania: Experimental and theoretical insights, *J. Alloys Compd.*, 2023, **960**, 170722.
31 T. Abdullah, S. I. Shamsah, I. A. Shaaban, M. Akhtar and S. Yousaf, Engineering energy storage properties of rGO based Fe2O3/CuO/PANI quaternary nanohybrid as an ideal electroactive material for hybrid supercapacitor application, *Synth. Met.*, 2023, **299**, 117472.
32 S. Yousaf, M. Aadil, S. Zulfiqar, M. F. Warsi, P. O. Agboola, M. F. A. Aboud and I. Shakir, Hierarchically porous CuO microspheres and their r-GO based nanohybrids for electrochemical supercapacitors applications, *J. Mater. Res. Technol.*, 2020, **9**(6), 14158–14167.
33 S. Kumar, A. K. Kaliamurthy, K. Kavu, S. Paramasivam, T. Appadurai, A. Sonachalam and S. Lee, Effect of fluoride (CoF2) based electrode material for high energy and power density asymmetric flexible supercapacitors, *J. Energy Storage*, 2024, **87**, 111460.
34 K. M. Anilkumar, M. Manoj, B. Jinisha, V. S. Pradeep and S. Jayalekshmi, Mn3O4/reduced graphene oxide nanocomposite electrodes with tailored morphology for high power supercapacitor applications, *Electrochim. Acta*, 2017, **236**, 424–433.
35 S. Kumar, A. K. Kaliamurthy, K. Kavu, S. Paramasivam, T. Appadurai, A. Sonachalam and S. Lee, Effect of fluoride (CoF2) based electrode material for high energy and power density asymmetric flexible supercapacitors, *J. Energy Storage*, 2024, **87**, 111460.
36 Q. Wu, T. He, Y. Zhang, J. Zhang, Z. Wang, Y. Liu and F. Ran, Cyclic stability of supercapacitors: materials, energy storage mechanism, test methods, and device, *J. Mater. Chem. A*, 2021, **9**(43), 24094–24147.